Modeling of Synchronous Reluctance Motors by Analytical and Finite Element Approaches for Electric Vehicle Applications

Hung Bui Duc*, Dung Dang Chi, Phi-Chi Do, Vuong Dang Quoc

Abstract—The design and analysis of synchronous reluctance motor (SynRM) with a distributed type winding is an alternative to replace the permanent magnet synchronous motors (PMSM), which is commonly used in electric vehicle applications. The use of a SynRM eliminates the need for permanent magnets (PMs), reducing the dependence on rare earth materials and potentially lowering costs. In this paper, there are two approaches: a new approach of step-skewing rotor (SSR) is proposed to improve eletromagnetic parameters such as minimization of the active volume, maximization of the output power and reduction of the torque ripple of the SynRM. Then, a finite element technique is developed to analyse and simulate the distribution of magnetic flux and map efficiency of the proposed SynRM. Additionally, the paper has also investigated the distribution of temparature and machnical stress in the region of flux barries of the rotor.

Index Terms—Synchronous reluctance motor (SynRM), torque ripple, step-skewing rotor, analytical model, finite element method.

1. Introduction

NOWADAYS, due to the highly reliability and efficiency compared with other machines, the synchronous reluctance motors (SynRMs) (Fig. 1) are used widely for different applications such as dry or wet conditions as well as in electric vehicle applications [1], [2]. But, these machines also have some inherent setbacks that need to be addressed. One of the significant challenges of SynRMs is the loss in the rotor winding, which can significantly affect directly to the efficiency and performance.

In order to address this challenge, many researchers have recently proposed different solutions to optimize the motor design and improve the performances of the SynRM [3]- [10]. Reference [3], an analytical model was presented for the transversally laminated anisotropicrotor to implemente on a previously designed SynRM. In this study, the electromagnetic torque and inductances investigated with different input currents. Reference [4], the modeling of SynRM with 2-D MEC takes into account the non-linear effects of the magnetic core and uses a magnetic circuit model to simulate the electromagnetic performance. This model was used to calculate various performance criteria and to evaluate the motor performance under different operating conditions. Reference [5], the efficiency of the line start permanent magnet (PM) SynRMs was improved via the optimal arrangements of PMs on rotor. In this paper, the demagnetization and skewed slots and effects was taken into account. Reference [6], the parameters of the SynRM were analysed by a magnetic equivalent circuit model. The model includes the variation of the air-gap flux with rotor position, which is crucial for accurate predictions of the motor behavior. The analysis of the torque characteristics of an example SynRM demonstrates the model ability to predict the motor performance under different operating conditions. Reference [7], an optimization method was developed for the SynRM to improve the torque ripple and THD in phase voltage. Reference [8], the paper provided insights into the design of the SynRMs with single tooth windings. The paper also investigated the impact of inter-segment air-gaps, torque ripple, and axial fringing on motor performance, providing useful information for motor designers and researchers. Reference [9], the paper proposed a novel type of rotor structure for medium speed SynRMs to test with a common rotor structure.

Reference [10], an accurate method was presented to defined equivalent circuit parameters of the SynRM. The proposed method was based on phase currents and voltages analysis at low slip operation, and it was verified by experimental and simulation studies.

In this paper, a new approach of step-skewing rotor (SSR) is proposed to improve electromagnetic param-

Hung Bui Duc is with School of Electrical and Electronic Engineering, Hanoi University of Science and Technology.

Dung Dang Chi is with School of Electrical and Electronic Engineering, Hanoi University of Science and Technology.

Phi-Chi Do is with Electrical-Electronic Engineering Cao Thang Technical College.

Vuong Dang Quoc is with School of Electrical and Electronic Engineering, Hanoi University of Science and Technology.

**Corresponding author: Hung Bui Duc (e-mail: hungbuiduc@hust.edu.vn)*

Manuscript received March 15, 2023; revised April 07, 2023; accepted May 05, 2023.
Digital Object Identifier 10.31130/jst-ud.2023.085ICT

eters and reduce torque ripple of the SynRM. Then, a finite element method (FEM) is developed to analyse and simulate the distribution of magnetic flux and map efficiency of the proposed SynRM. The development of these two approaches is validate on the practical SynRM of 150 kW with 48-slots/8-poles distributed winding for electric applications. The target specifications is referred to Volkwagen ID 150 kW as shown in Fig. 2.

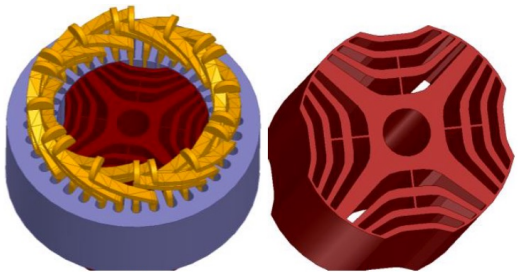

Fig. 1: 3D model of SynRM with a flux guided rotor [1].

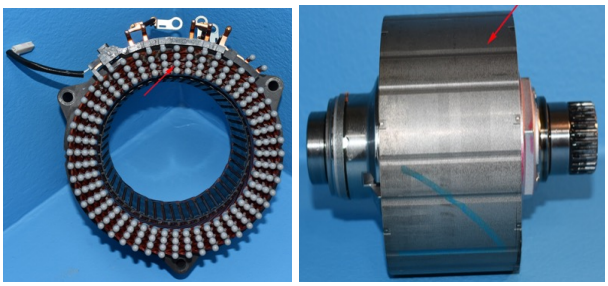

Fig. 2: Stator and rotor cores of Volkwagen ID3.

2. Theory background for analytical approach

The electromagnetic torque (T) is expressed as [11]:

$$T = \frac{1}{2}\pi D^2 L_r \sigma, \tag{1}$$

where D is the outer rotor diameter, L_r is the rotor length and σ is a factor (which can be defined from 0.8 to 1.25). At the steady-state, in the d, q-axis, the electromagnetic torque (T) is then defined as [13]- [16]

$$T_e = \frac{3}{2}p[\phi_M i_q + (L_d - L_q) i_d i_q], \tag{2}$$

where ϕ_M is the magnetic flux due linked to the armature winding, the i_d and i_q are respectively the d- and q-axis; the L_d and L_q are the d- and q-inductance. The voltage equations are written as [12]- [14].

$$v_d = Ri_d - \omega_q i_q, \tag{3}$$

$$v_d = Ri_d - \omega_q i_q, \tag{4}$$

where R is the stator resistance and inductances.

A three phase SynRM of 150 kW, with 48 slots/8 poles is now considered to validate the developed theory. The cross-section of stator and rotor section with several flux barriers is presented in Fig. 3. The PMs will be inserted into these cavities. In the stator part, the slots of stator are inserted by distributed windings with double-layer. The set of parameters of X_j (j = 1 to 9) is presented to do an optimization procedure as given in Table 1. This table presents minimum and maximum ranges of design variables. In addition, the other parameters such as outer stator diameter, magnet length, air gap, magnet angles and slot depth will be varied in a discrete way. In order to obtain the high performance, the irreversible demagnetization should be minimized and other parameters need to be also optimized with main constraints of the efficiency $\geq 91\%$ and torque ripple $\leq 5\%$.

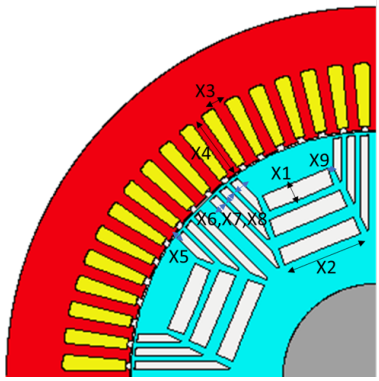

Fig. 3: Stator and rotor cores of Volkwagen ID3.

TABLE 1: Minimum and Maximum ranges of design variables.

Parameters	Discrete variables	min	max	step
Thickness layer 1	X1	1	4	0.5
Thickness layer 2	X6, X7, X8	0.5	2	0.1
Bridge thickness (mm)	X5	0.5	2	0.1
Tooth depth (mm)	X4	1.5	4.5	0.1
Tooth width (mm)	X3	18	20	0.2
Layer width	X2	7	10	0.2
Post thickness	X9	1	2	0.1

An optimization procedure is required to iteratively update and identify the set of motor parameters by making a trade-off between the different parameters of the machine.

In order to reduce the cogging torque, torque ripple and harmonic components of back electromotive force (EMF), a method of step-skewing rotor (SSR) is proposed. In this approach, a motor with a SSR and another with a slot-skewed stator is analysed to compare the performance of each motor. Fig. 4 shows the principle of the SSR with different angles.

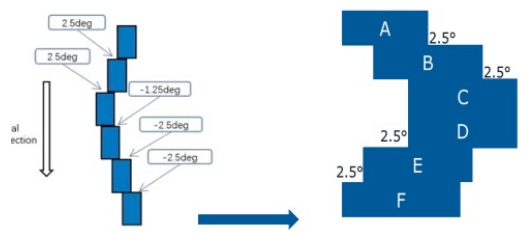

Fig. 4: Step skewing rotor.

By this way, the harmonics of back EMF will be reduced. The step-skew factors of harmonics are [15]:

$$k_{skew\,pole\,v} = \frac{\sin(\frac{n \cdot v \cdot a}{2(n-1)})}{n \sin(\frac{v \cdot a}{2(n-1)})} \tag{5}$$

where n is the number of steps, α is the step skew angle and v is the order number of harmonic components. As mentioned in [4], the reduction factor of PM torque of step-skewed motor is given as

$$k_{T\,skew\,pole\,PM} = \frac{\sin(\frac{n \cdot a}{2(n-1)})}{n \sin(\frac{\alpha}{2(n-1)})} \tag{6}$$

and the reduction factor of reluctant torque is

$$k_{T\,skew\,pole\,RE} = \frac{\sin(\frac{n \cdot a}{(n-1)})}{n \sin(\frac{\alpha}{(n-1)})} = k_{T\,skew\,pole\,PM} \cos\frac{\alpha}{2} \tag{7}$$

The torque is finally expressed as [15]- [19]:

$$T = \frac{3}{2} pn\phi_M I_s k_{T\,skew\,pole\,PM} \sin\beta + \frac{3}{4} pn I_s^2 (L_d - L_q) k_{T\,skew\,pole\,RE} \sin 2\beta \tag{8}$$

where β is the mechanical angle and Is is the stator current. Based on the equation (7), it can be seen that the step number and step skew angle affect drirectly to the torque and the power density of motor.

In traction applications, to reduce the torque ripple and avoid producing extra noise, an objective function with the average torque should be considered. The objective function is expressed as [20]- [23]:

$$f = W_1 (T_{av(norm)} - G_1)^2 + W_2 (T_{ripple(norm)} - G_2)^2 \tag{9}$$

where W_1 and W_2 are respectively the weight value of the average torque and the torque ripple; G_1 and G_2 are respectively the desired value of the normalized average torque and torque ripple; T_{av} and T_{ripple} are the average torque and torque ripple, respectively. The torque ripple is defined as:

$$T_{ripple} = \frac{T_{max} - T_{min}}{T_{av}} \tag{10}$$

In this study, G_1 and G_2 are chosen arbitrarily, that is G_1 = 10 and G_2 = 1. For that, the normalized average torque and torque ripple are defined to attain the values between 1 and 10 during the optimization procedure. Then they have [21], [22]:

$$T_{av(norm)} = 1 + \frac{(T_{av} - 150)9}{200} \tag{11}$$

$$T_{ripple(norm)} = 1 + \frac{(T_{ripple} - 0.05)9}{0.17} \tag{12}$$

Based on the theorical background, the main/geometry prameters of the proposed motor are given in Table 2.

The distribution of torque ripple obtained from the conventional (initial) and optimal solutions is shown in Fig. 5. For the initial solution, the value approximately varies from 180 $N.m$ up to 210 $N.m$, and from 180 $N.m$ to 190 $N.m$ for the optimal solution. This means that the torque ripple of the initial model is higher than 10% comparted to the optimal model.

TABLE 2: Geometry parameters.

No	Parameters
1	48 slots, 8 poles
2	Shaft diameter = 60 mm
3	Rotor outer diameter = 142.8 mm
4	Stator inner diameter = 144.2 mm
5	Air gap length = 0.7 mm
6	Stator stack length = 140 mm
7	Rotor stack length = 141.6 mm
8	Average stack = 140.8 mm

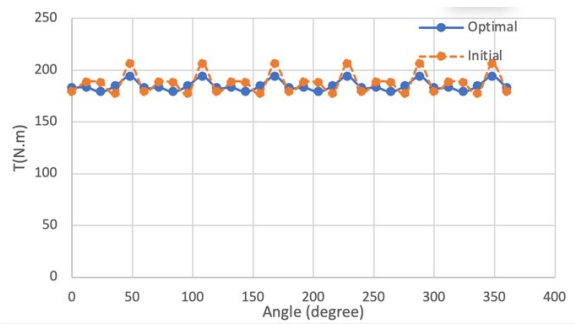

Fig. 5: Torque ripple distribution.

The comparison of electromagnetic results between initial and optimal models are given in Table 3.

TABLE 3: Comparison of Electromagnetic results between initial and optimal models.

Parameters	Optimal model	Initial model	Unit
Maximum torque	217.96	217.28	Nm
Average torque	188.25	171.35	Nm
Torque Ripple	14.127	17.997	Nm
Torque Ripple %	7.5717	10.634	%
Speed limit	12536	11347	rpm
Electromagnetic Power	97687	88617	W
Input Power	$1.03.10^5$	93612	W
Total Losses	8610.7	8686.9	W
Output Power	94113	84925	W
Shaft Torque	179.74	162.19	Nm
System efficiency	91.618	90.72	%

3. Finite element approach

The maxwell equations and behavior laws are written in Euclidean space R^3 [10]:

$$\text{rot}\,\boldsymbol{H} = \boldsymbol{J}_s,\ \text{rot}\,\boldsymbol{E} = -\partial_t \boldsymbol{B}, \text{div}\,\boldsymbol{B}_n = 0 \tag{13a-b-c}$$

$$\boldsymbol{B} = \mu_n \boldsymbol{H}\ ,\ \boldsymbol{J} = \sigma \boldsymbol{E} \tag{14a-b}$$

Where:

- $\boldsymbol{H}$: magnetic field (A/m),
- $\boldsymbol{B}$: magnetic flux density (T),
- $\boldsymbol{J}_s$: electric current density (A/m2),
- $\boldsymbol{J}$: electric eddy current (A/m2),

- $\boldsymbol{E}$: electric field (V/m),
- σ: electric conductivity (S/m).
- μ: relative permeability.

The boundary conditions (BCs) are given as

$$\boldsymbol{n} \cdot \boldsymbol{B}|_{\Gamma_e} = 0\,,\ \boldsymbol{n} \times \boldsymbol{H}|_{\Gamma_h} = 0\,, \tag{15a-b}$$

where n is the unit normal exterior to Ω [10].

Based on the Ampere equation 13 a) and the constitutive law 14 a) , the weak formulation is defined as [10], [11]:

$$\oint_{\Omega} \mu^{-1}\boldsymbol{B} \cdot \text{rot}\, \boldsymbol{A} d\Omega + \oint_{\Omega} \sigma \boldsymbol{E} \cdot \boldsymbol{A}' d\Omega_c + \int_{\Gamma_h} \boldsymbol{n} \times \boldsymbol{H} \cdot \boldsymbol{A}' d\Gamma_h = \oint_{\Omega} \boldsymbol{J}_s \cdot \boldsymbol{A}' d\Omega_s, \boldsymbol{A}' \in \boldsymbol{H}^1_h(\text{rot};\Omega), \tag{16}$$

where $\boldsymbol{H}^1_h(\text{rot};\Omega)$ is the function space containing the test function $\boldsymbol{A}'$ defined in studied domain Ω. The field $\boldsymbol{B}$ is defined via the vector potential ($\boldsymbol{A}$), i.e,

$$\boldsymbol{B} = \text{rot}\, \boldsymbol{A}, \tag{17}$$

From the equations (17) and (13 c), the field $\boldsymbol{E}$ is defined via an electric scalar potential (v), that is

$$\boldsymbol{E} = -j\omega \boldsymbol{A} - \text{grad}\, v \tag{18}$$

The field $\boldsymbol{E}$ in (17) is defined via an electric scalar potential (v).

4. Numerical simulation

Based on the theory developed of the FEM in Section 3, in this section, the parameters given in Table 2 by the analytical approach are applied to compute and simulate and by the FEM. The magnetic flux distribution on rotor and stator is presented in Fig. 6. It can be seen that the maximum magnetic flux density is 2.045T.

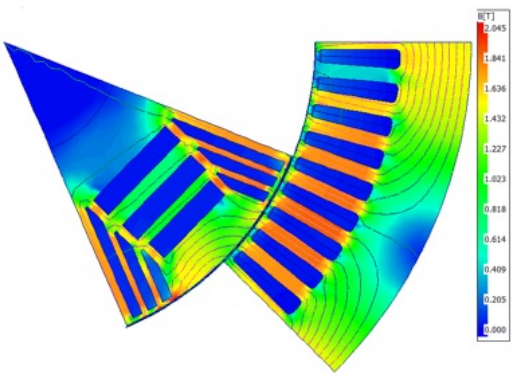

Fig. 6: Magnetic flux distribution on rotor and stator.

Fig. 7 shows the map of the relationship between torque and speed. The continuous torque requirement of 120 $N.m$ is exceeded up to 8000 rpm, whereas the maximum efficiency point is 96% for the maximum torque of 230 $N.m$.

The map of the relationship between output power and speed is pointed out in Fig. 8. The output power of 150 kW is available between 6000 rpm to 8000 rpm.

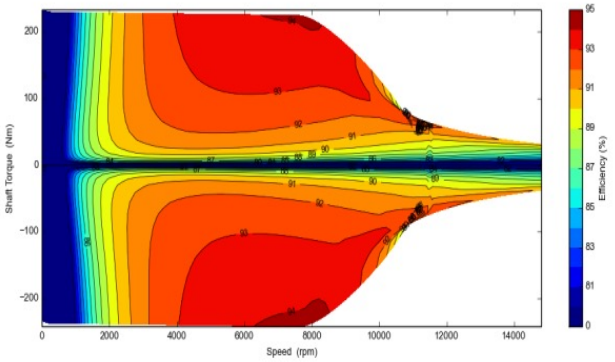

Fig. 7: Map of the relationship between torque and speed.

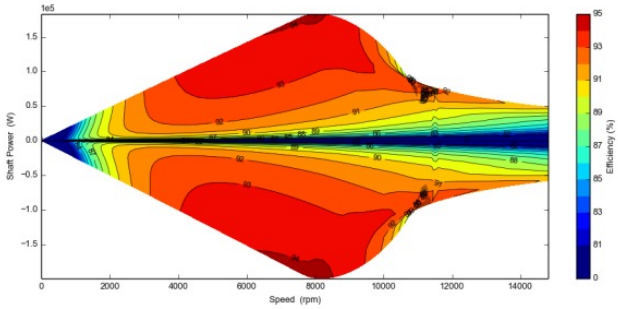

Fig. 8: Map of the relationship between output power and speed.

The continuous peak power is close to the 200 kW for the efficiency of 95%.

The SynRM can be operated with the thermal limits for all speed range is shown in Fig. 9. It can be seen that after 10 duty cycles (5,960 sec), the temperature of stator winding with yellow curves reaches a maximum degree of 94.6^0C. In this region, the temperature is slightly higher (transient peak 109.5^0C), but this value does not directly influence on the performance of the motor.

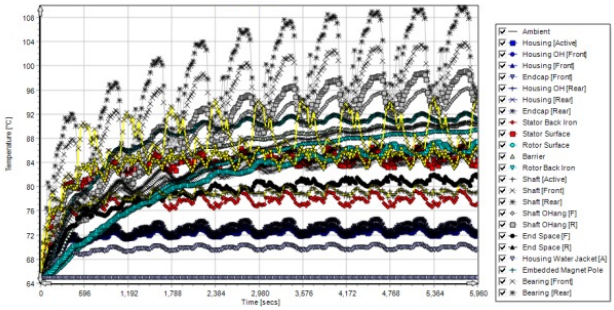

Fig. 9: Temperature distribution with the transient case.

The map region of mechanical stress is also presented in Fig. 10. The mechanical stress in this region is 455 MPa. This stress appears on the surface of flux barriers, which can be observed via the mesh as shown in left hand side of Fig. 10. These regions can be adapted via dedicated mechanical design.

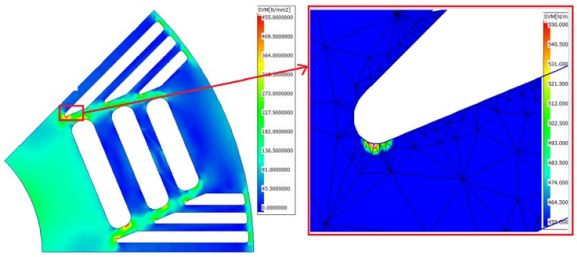

Fig. 10: Map region of mechanical stress.

5. Conclusion

Two approaches of this paper have been successfully presented. The multi-objective function has been proposed to obtain the optimal solutions such as the everage torque, torque ripple, output power and efficiency. Then, the FEM has been also used to show the maps of the distribution of magnetic flux density, shaft torque and output power. The distribution of the temperature and mechanical stress are finally presented to show the areas with the high temperature and stress. Based on the obtained results, it will help manufactures and designers to change of the design variables. The obtained results in this paper were performed via the ANSYS Maxwell software (Electronics Desktop V19. R1) and MotorCad software. In the future work, the developed method can be extended for considering the addition of permanent magnet into the flux barriers to improve the efficiency and power factor of the SynRM.

Acknowledgment

The authors also gratefully acknowledges Quy Nhon University, created favorable conditions for the authors to use the copyright-supported Ansys software program to compute and simulate the practical problem in this research. This software is the package belonging to ANSYS Electronics Desktop V19. R1.

References

[1] Toomas Rassõlkin, Anton, "Analytical modelling of synchronous reluctance motor including nonlinear magnetic condition," *IET Electric Power Applications.*, Vol.16. pp. 511-524, 2022, Doi=https://www.mdpi.com/1996-1073/11/6/1385.

[2] Mohananarajah, Thushanthan Rizk, Jamal Nagrial, M. Hellany, Ali, "Finite Element Analysis and Design Methodology for High-Efficiency Synchronous Reluctance Motors," *Electric Power Components and Systems.*, Vol. 46. pp. 1-16, 2018 Doi=0.1080/15325008.2018.1489436.

[3] Burak Solak, Tunahan Sapmaz, Yasemin Oner, "Non-linear analytical model for synchronous reluctance machine," *Journal of Magnetism and Magnetic Materials.*, Vol. 571, pp. 170570, 2023. Doi=https://doi.org/10.1016/j.jmmm.2023.170570.

[4] Peyman Naderi, "Cage-rotor induction motor inter-turn short circuit fault detection with and without saturation effect by MEC model. ISA Transactions," *ISA Transactions.*, Vol. 64, pp. 216-230, 2023. Doi=https://doi.org/10.1016/j.isatra.2016.05.014.

[5] T. H. Manh, D. B. Minh, T. P. Minh, and V. D. Quoc, "Investigation of the Influence of Skewed Slots and Demagnetization Effects to Line Start Permanent Magnet Assistance Synchronous Reluctance Motors," *Eng. Technol. Appl. Sci. Res.*, Vol. 13, no. 1, pp. 9807–9811, Feb. 2023. Doi=https://doi.org/10.48084/etasr.5307.

[6] Jayarajan, R.; Fernando, N.; Mahmoudi, A.; Ullah, N. "Magnetic Equivalent Circuit Modelling of Synchronous Reluctance Motors," *Energies*, Vol. 15, 4422, 2022. Doi=https://doi.org/10.3390/en15124422.

[7] Zhang, G.; Tao, J.; Li, Y.; Hua, W.; Xu, X.; Chen, Z. "Magnetic Equivalent Circuit and Optimization Method of a Synchronous Reluctance Motor with Concentrated Windings," *Energies*, Vol. 15, 1735, 2022. Doi=https://doi.org/10.3390/en15051735.

[8] C. M. Donaghy-Spargo, B. C. Mecrow and J. D. Widmer. "Electromagnetic Analysis of a Synchronous Reluctance Motor With Single-Tooth Windings," in *IEEE Transactions on Magnetics.*, Vol. 53, no. 11, pp. 1-7, Nov. 2017, Art no. 8206207. Doi=doi: 10.1109/TMAG.2017.2700896.

[9] J. Kolehmainen. "Synchronous Reluctance Motor With Form Blocked Rotor," *IEEE Trans. on energy conversion.*, Vol. 25, no. 2, pp. 450-456, 2010. Doi=10.1109/TEC.2009.2038579.

[10] Łyskawinski, Wiesław, Cezary Jędryczka, Dorota Stachowiak, Piotr Łukaszewicz, and Michał Czarnecki. "Finite element analysis and experimental verification of high reliability synchronous reluctance machine," Eksploatacja i Niezawodność – Maintenance and Reliability., Vol. 24, no. 2, pp. 386-393, 2022. Doi=10.17531/ein.2022.2.20.

[11] N.Bianchi, S. Bolognani , D.Bon, M. Dai Pré. "Design for Torque Ripple Reduction in Synchronous Reluctance and PM-Assisted Synchronous Reluctance Motors," *IEEE Trans. on Ind. Appl.*, Vol. 45, No.3, pp. 921-928, 2009. Doi=doi: 10.1109/TIA.2009.2018960.

[12] W. Fei, P. C. K. Luk, D. -M. Miao and J. -X. Shen. "Investigation of Torque Characteristics in a Novel Permanent Magnet Flux Switching Machine With an Outer-Rotor Configuration," in *IEEE Transactions on Magnetics.*, vol. 50, no. 4, pp. 1-10, 2014. Doi=10.1109/TMAG.2013.2288219.

[13] Y. Fan, L. Zhang, J. Huang and X. Han. "Design, Analysis, and Sensorless Control of a Self-Decelerating Permanent-Magnet In-Wheel Motor," in *IEEE Transactions on Industrial Electronics.*, vol. 61, no. 10, pp. 5788-5797, 2014. Doi=110.1109/TIE.2014.2300065.

[14] S. O. Edhah, J. Y. Alsawalhi and A. A. Al-Durra. "Multi-Objective Optimization Design of Fractional Slot Concentrated Winding Permanent Magnet Synchronous Machines," in *IEEE Access*, vol. 7, pp. 162874-162882, 2019. Doi=10.1109/ACCESS.2019.2951023.

[15] J. H. Lee, J. -W. Kim, J. -Y. Song, Y. -J. Kim and S. -Y. Jung. "A Novel Memetic Algorithm Using Modified Particle Swarm Optimization and Mesh Adaptive Direct Search for PMSM Design," in *IEEE Transactions on Magnetics.*, vol. 52, no. 3, pp. 1-4, 2016. Doi=10.1109/TMAG.2015.2482975.

[16] S. Zhang, W. Zhang, R. Wang, X. Zhang and X. Zhang. "Optimization design of halbach permanent magnet motor based on multi-objective sensitivity," in CES Transactions on Electrical Machines and Systems," in *CES Transactions on Electrical Machines and Systems.*, vol. 4, no. 1, pp. 20-26, 2020. Doi=10.30941/CESTEMS.2020.00004.

[17] L. Zhai, T. Sun and J. Wang. "Electronic Stability Control Based on Motor Driving and Braking Torque Distribution for a Four In-Wheel Motor Drive Electric Vehicle," in CES Transactions on Electrical Machines and Systems," in *IEEE Transactions on Vehicular Technology.*, vol. 65, no. 6, pp. 4726-4739, 2016. Doi=10.1109/TVT.2016.2526663.

[18] X. Zhu, Z. Shu, L. Quan, Z. Xiang and X. Pan. "Design and Multicondition Comparison of Two Outer-Rotor Flux-Switching Permanent-Magnet Motors for In-Wheel Traction Applications," in *IEEE Transactions on Industrial Electronics.*, vol. 64, no. 8, pp. 6137-6148, 2017. Doi=10.1109/TVT.2016.2526663.

[19] Y. Wang, H. Fujimoto and S. Hara. "Driving Force Distribution and Control for EV With Four In-Wheel Motors: A Case Study of Acceleration on Split-Friction Surfaces," in *IEEE Transactions on Industrial Electronics.*, vol. 64, no. 4, pp. 3380-3388, 2017. Doi=10.1109/TIE.2016.2613838.

[20] Chang-Chou Hwang and Y. H. Cho. "Effects of leakage flux on magnetic fields of interior permanent magnet synchronous motors," in *IEEE Transactions on Magnetics*, vol. 37, no. 4, pp. 3021-3024, 2001. Doi=10.1109/20.947055.

[21] Ilka, Reza Alinejad-Beromi, Yousef Yaghobi, Hamid. "Techno-economic Design Optimisation of an Interior Permanent Magnet Synchronous Motor by Multi-objective approach," *IET Electric Power Applications.*, vol. 12, no. 7, pp. 772-778, 2018 Doi=https://doi.org/10.1049/iet-epa.2018.0150.

[22] G. Hong, T. Wei and X. Ding. "Multi-Objective Optimal Design of Permanent Magnet Synchronous Motor for High Efficiency and High Dynamic Performance," in *IEEE Access*, vol. 6, pp. 23568-23581, 2018. Doi=10.1109/ACCESS.2018.2828802.

[23] S. -K. Cho, K. -H. Jung and J. -Y. Choi. "Design Optimization of Interior Permanent Magnet Synchronous Motor for Electric Compressors of Air-Conditioning Systems Mounted on EVs and HEVs," in *IEEE Transactions on Magnetics*, vol. 54, no. 11, pp. 1-5, Nov. 2018, Doi=10.1109/TMAG.2018.2849078.

Hung Bui Duc received the PhD degree in 2000 from Department of Electrical Engineering, Hanoi University of Science and Technology. He is currently working as a team leader of electrical machines's group, and also a lecturer of Department of Electrical Engineering, School of Electrical Engineering, Hanoi University of Science and Technology, no1 Dai Co Viet Street, Ha Ba Trung District, Ha Noi. He can be contacted at e-mail: hung.buiduc@hust.edu.vn.

Dung Dang Chi is a deputy of Office Head, School of Electrical and Electronic Engineering, Hanoi University of Science and Technology. He received the MS.C degree in 2003 from Department of Electrical Engineering, Hanoi University of Science and Technology. He can be contacted at e-mail: dung.dangchi@hust.edu.vn.

Phi-Chi Do is a Dean of Electrical Electronic Engineering Cao Thang Technical College, Ho Chi Minh city, Vietnam. PhD, Hanoi University of Science and Technology in 2016. He is Studying in Electrical Engineering, electrical installation skills, design install a Solar or lighting system; ability to operate, assemble, maintain electrical equipment, electrical systems and solve problems related to electricity and equipment in the production. He can be contacted at e-mail: dochiphi@caothang.edu.vn.

Vuong Dang Quoc received his PhD degree in 2013 from the Faculty of Applied Sciences at the University of Liege in Belgium. After that he came back to the Hanoi University of Science and Technology in September 2013, where he is currently working as a lecturer of Department of Electrical and Electronic Equipment, School of Electrical Engineering, Hanoi, University of Science and Technology. His research domain encompasses modeling of electromagnetic systems by coupling of subproblem method with application to thin shell models. E-mail: vuong.dangquoc@hust.edu.vn.